Model Predictive Saturation Controller-Based Direct Torque Control of Permanent-Magnet Synchronous Machines

Matthew Penne, Wei Qiao, Liyan Qu, and Lizhi Qu
Department of Electrical and Computer Engineering
Univeristy of Nebraska-Lincoln
Lincoln, NE 68588-0511 USA
mpenne2@unl.edu; wqiao3@unl.edu; lqu2@unl.edu,
lizhi.qu@huskers.unl.edu

Jiyao Wang and Silong Li
eDrive Applications
Ford Motor Company
Dearborn, MI 48120 USA
jwang288@ford.com, sli141@ford.com

***Abstract*—The conventional direct torque control (DTC) for permanent-magnet synchronous machines (PMSMs) uses hysteresis comparators to determine a single voltage vector per control period based on the torque and stator flux tracking errors. The saturation controller-based DTC (SDTC) is a duty cycle DTC strategy that uses nonlinear adaptive midpoint saturation controllers to determine the duration of two active voltage vectors and a zero voltage vector for each control period. A new voltage vector table and the outputs of the saturation controllers determine the duty cycle for each phase. This paper proposes a novel model predictive SDTC (MPSDTC) strategy for PMSMs with low sampling frequency, fast transient response, and low steady-state torque and flux ripples. The MPSDTC uses a computational model of the SDTC to predict the torque, stator flux linkage, current, etc. of the PMSM in the immediate next control period and possibly future control periods. The predicted values are then used to form a cost function that is minimized to find the optimized saturation controller outputs. The MPSDTC has better transient and steady state torque characteristic than the traditional field-orientated control (FOC) or the SDTC.**

Keywords—Model predictive control (MPC), permanent-magnet synchronous machine (PMSM), saturation direct torque control (SDTC)

I. INTRODUCTION

Direct torque control (DTC) is a popular method of high-performance control of electric machines. Compared to the more commonly used field-orientated control (FOC) methods, DTC uses the torque and stator flux linkage of the machine as the control variables instead of the *d*- and *q*-axis currents. Conventional DTC has fast transient response and does not require a position sensor [1]. Improving DTC has been a popular research topic since its creation.

In conventional DTC, a switching table determines which voltage vector will be applied to the inverter driven PMSM according to the outputs of a torque and a stator flux hysteresis controllers. The structure of conventional DTC is shown in Fig. 1. Since the control strategy is implemented on digital hardware (DSP or FPGA), the performance of DTC is affected by the sampling frequency of the controller. Lowering the sampling frequency of DTC results in large steady state ripples of the torque, stator flux linkage, and current [1], [2]. Higher sampling frequencies can improve performance but increase the cost of the controlling hardware.

Much research has been conducted in reducing the steady state torque and flux ripples of DTC. One option is to increase the number of possible voltage vectors by using a multi-level inverter, but this significantly increases hardware costs [3]. Duty cycle DTC (DDTC) uses modulation to implement the given active voltage vector for a portion of the control period [4]. DDTC can reduce steady state torque and flux ripple, but commonly has a mean offset from the given torque and flux reference values, making DDTC unfit for precise torque control. Saturation DTC (SDTC) is a form of DDTC [5], [6]. SDTC uses nonlinear adaptive midpoint saturation controllers and an updated switching table to determine the duty cycle of the inverter. Model predictive control (MPC) is used in [7] to reduce DTC steady state ripple. MPC is found to further improve the steady state ripple of DDTC in [8]. MPC increases the complexity and computation time of DTC.

This paper proposes a model predictive SDTC (MPSDTC) strategy, which applies the MPC principle to find the optimized outputs of the SDTC controllers according to the given cost function for the specified prediction horizon. A novel cost function includes maximum torque per ampere tracking and steady state torque ripple minimization in addition to conventional torque and flux tracking. Simulation and experimental results show the transient and steady state performance improvements of MPSDTC over SDTC and conventional FOC.

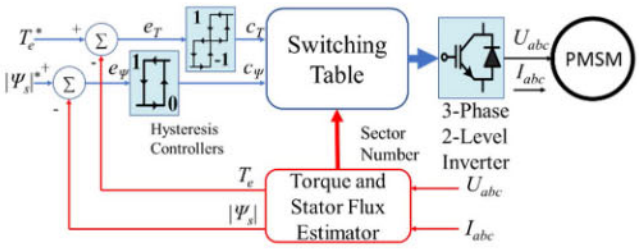

Fig. 1. Conventional DTC schematic.

This work was supported in part by Nebraska Public Power District through the Nebraska Center for Energy Sciences Research and in part by Ford Motor Company.

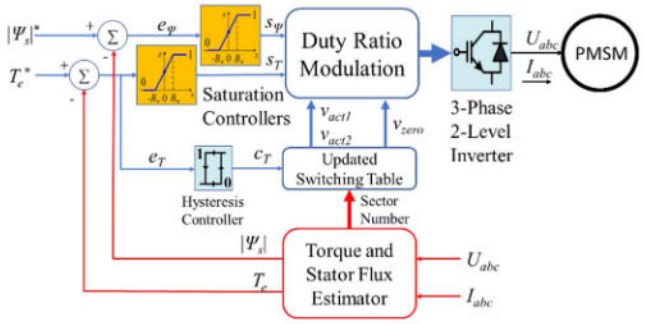

Fig. 2. SDTC schematic.

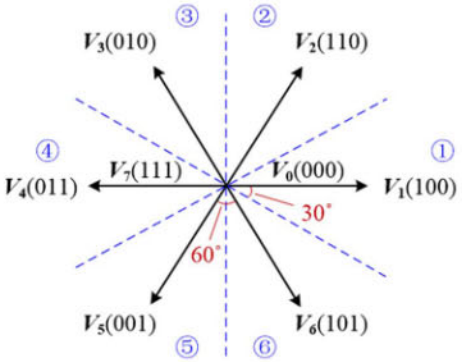

Fig. 3. Inverter voltage vectors and segment of sectors in the $\alpha\beta$ reference frame.

II. Saturation Direct Torque Control

A schematic diagram of SDTC is shown in Fig. 2. The traditional hysteresis controllers are replaced with saturation controllers and the conventional switching table is replaced with a modified switching table and duty ratio modulation.

In SDTC, the duty ratio applied to the inverter is determined from a multiple voltage vectors, instead of the one used in DDTC. The additional hysteresis output c_T indicates transient or quasi-steady state situations to provide additional information for the new switching table. SDTC has a fast transient response like DTC, but has much lower steady state torque and flux ripple

A. Nonlinear Adaptive Midpoint Saturation Controller

The output of the adaptive midpoint saturation controllers is defined in (1) where x is the input to the comparator, B_w is the bandwidth of the saturation controller, and d^* is the adaptive midpoint defined in (4) and (5). Using saturation controllers provides continuous values from zero to one instead of discreate values produced by traditional hysteresis controllers.

$$sat(x, B_w) = \begin{cases} 0.5(sgn(x)+1), & |x| \geq B_w \\ 0.5\dfrac{x}{B_w} + d^*, & |x| < B_w \end{cases} \quad (1)$$

B. Modified Switching Table

The possible voltage vectors and the electric sectors for a three-phase two-level inverter are shown in Fig. 3. The proposed switching table is shown in Table I. From this table, two active voltage vectors v_{act1} and v_{act2} and a zero vector v_{zero} will be selected each switching period. The inputs of the switching table are the sector number of the stator flux vector location as shown in Fig. 3, and the output of the additional hysteresis controller, c_T. The value of c_T for the kth (current) time step is defined in (2) where e_T is the output of the torque comparator and B_w is the bandwidth of the hysteresis controller.

$$c_T[k] = \begin{cases} 1, & e_T[k] > B_w \\ 0, & e_T[k] < -B_w \\ c_T[k-1], & |e_T[k]| < B_w \end{cases} \quad (2)$$

If $c_T[k]$ is 1, then the torque of the machine is less than the reference torque by more than the torque bandwidth, so active voltage vectors that will increase the torque will be applied. If $c_T[k]$ is 0, then the torque of the machine is greater than the reference torque by more than the torque bandwidth, so active voltage vectors that will decrease the torque will be applied.

Table I. Updated Switching Table

Sector	1	2	3	4	5	6
$c_T = 1$	V_2(110) V_3(010) V_7(111)	V_3(010) V_4(011) V_7(111)	V_4(011) V_5(001) V_7(111)	V_5(001) V_6(101) V_7(111)	V_6(101) V_1(100) V_7(111)	V_1(101) V_2(100) V_7(111)
$c_T = 0$	V_6(101) V_5(001) V_7(111)	V_1(100) V_6(101) V_7(111)	V_2(110) V_1(100) V_7(111)	V_3(010) V_2(110) V_7(111)	V_4(011) V_3(010) V_7(111)	V_5(101) V_4(100) V_7(111)

The modified switching table is defined in Table I. Using the voltage vectors determined from Table I, c_T, s_T and s_ψ, the duty cycle D is defined as follows.

$$\boldsymbol{D} = \begin{cases} s_T[s_\psi * \boldsymbol{v_{act1}} + (1-s_\psi) * \boldsymbol{v_{act2}}] \\ \quad +(1-s_T) * \boldsymbol{v_{zero}}, & c_T = 1 \\ (1-s_T) * [s_\psi * \boldsymbol{v_{act1}} + (1-s_\psi) * \boldsymbol{v_{act2}}] \\ \quad +s_T * \boldsymbol{v_{zero}}, & c_T = 0 \end{cases} \quad (3)$$

where v_{act1}, v_{act2}, and v_{zero} are the three vectors selected from Table I. The resulting three elements of the duty cycle vector are the on time for each of the three phases of the inverter. Changing the applied zero voltage vector is explored in [6], and a constant zero vector of (111) will be used throughout this paper.

C. Torque and Flux Adaptive Midpoints

The adaptive midpoints of the saturation controllers are used to make the output of (1) symmetric about the midpoint of the discrete change in the stator flux linkage vector. For the torque saturation controller, the midpoint is derived from the back electromagnetic force of the PMSM and the voltage drop of the armature resistance [5]. The adaptive midpoint of the flux saturation controller is based on equaling the d-axis magnitudes of v_{act1} and v_{act2} as well as a slight speed offset [5]. The torque adaptive midpoint mitigates steady state torque tracking error, while the flux adaptive midpoint eliminates periodic flux pulses. The equation for the adaptive torque and flux midpoints are (4) and (5), respectively.

$$d_T^* = \frac{\sqrt{3} * \left(\omega_e[k] * \Psi_s[k] + R_s * |I_s[k]| * sgn(T_e)\right)}{V_{DC}[k]} \quad (4)$$

$$d_\Psi^* = 1 - \frac{3 * (\theta + 1.5\omega_e[k]T_s)}{\pi}, \quad \theta \in [-1.5\omega_e[k]T_s, \frac{\pi}{3} - 1.5\omega_e[k]T_s \quad (5)$$

where ω_e is the electrical angular speed, Ψ_s is the stator flux linkage, I_s is the stator current, R_s is the stator resistance, T_e is the electromagnetic torque, θ is the rotor position, and T_s is the control period.

III. Model Predictive Saturation Direct Torque Control

Model predictive control is a popular control method for systems with long control periods, like chemical processing and some kinds of finance. Advances in microprocessors have made it possible for MPC to be used for systems with very short control periods, like high performance motor drives. For motor control, traditional MPC calculates the predicted torque, flux, current, etc. resulting from each possible combination of voltage vector inputs [7]. MPC is often called receding horizon control because it repeatedly optimizes the system control inputs for a given number of future steps, the prediction horizon, at every new time step. The calculated output variables are used to form a cost function, which is then minimized. The terms in the cost function are multiplied by weights to represent their significance to the overall control strategy. The corresponding voltage vector in the immediate next step that produced the smallest cost function value is then implemented, and the process is repeated. If a MPC strategy calculates output variables of the immediate next step, and one future step it has a prediction horizon of one.

A. Torque, Current, and Flux Calculations

To improve the performance of SDTC and to limit the computation time of MPC, a novel method of MPSDTC is proposed and shown in Fig. 4. In the MPSDTC, there are two input variables: S_T and S_Ψ for every future time step predicted. The values of S_T and S_Ψ range from 0 to 1. A continuous control set version of MPC (CCS-MPC) is used to solve the optimization problem. The initial values of S_T and S_Ψ are calculated as in Section II, then additional values of S_T and S_Ψ are generated with a Gaussian curve about the initial calculated values. The optimization problem is solved using particle swarm optimization with a fixed number of iterations. This method only provides a local optimum but can be solved faster than searching the problem space for a global optimum.

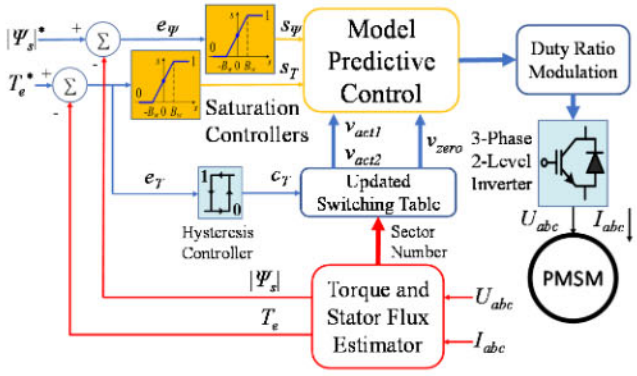

Fig. 4. Proposed MPSDTC schematic.

For each combination of input vectors, the resulting duty cycle is found from (3). Each of the three elements in the duty cycle are used to calculated time derivatives of torque, flux, and current. The time derivative equation of torque is shown in (6) [4],

$$\frac{dT_e}{dt} = \frac{-3p}{2}\left(\frac{1}{L_q} - \frac{1}{L_d}\right)\left(Im(U_s\Psi_s) - \omega_r Re(\Psi_s^2)\right) + \frac{3pR_s}{4}\left(\frac{1}{L_d^2} - \frac{1}{L_q^2}\right)Im(\Psi_s^2) - \frac{3p}{2L_d}\left(\frac{R_s}{L_d}Im(\Psi_s\Psi_r) + \omega_r Re(\Psi_s\Psi_r)\right) \quad (6)$$

where p is the number of pole pairs, L_d and L_q are the d- and q-axis stator inductances, respectively, U_s is the applied voltage vector, ω_r is the rotor angular speed, and Ψ_r is the flux linkage of the rotor permanent magnets. The discrete change in torque for v_{act1}, v_{act2}, and v_{zero} are calculated and multiplied by the corresponding on times. For example, if c_T is 1, then the discrete change in toque ΔT_e is given by (7).

$$\Delta T_e = T_s\left[s_T s_\Psi\left(\frac{dT_e}{dt}\Big|_{U_s=v_{act1}}\right) + (1-s_T)s_\Psi\left(\frac{dT_e}{dt}\Big|_{U_s=v_{act2}}\right) + (1-s_T)\left(\frac{dT_e}{dt}\Big|_{U_s=v_{zero}}\right)\right] \quad (7)$$

The standard equations for the time derivatives of the d- and q-axis currents are shown in (8),

$$\begin{cases}\frac{di_d}{dt} = \frac{(U_d - R_s i_d + \omega_e L_q i_q)}{L_d} \\ \frac{di_q}{dt} = \frac{(U_q - R_s i_q + \omega_e L_d i_d - \omega_e \Psi_r)}{L_q}\end{cases} \quad (8)$$

where i_d and i_q are the d- and q-axis stator currents, respectively, and U_d and U_q are the d- and q-axis components of the applied voltage vector, respectively [9]. These equations are used to find the discrete change in currents for each of the three applied vectors, like in (7). These changes in currents, Δi_d and Δi_q, are used to predicted d- and q-axis currents (9) and stator linkage fluxes (10) in the next time step.

$$\begin{cases}i_d[k+1] = i_d[k] + \Delta i_d \\ i_q[k+1] = i_q[k] + \Delta i_q\end{cases} \quad (9)$$

$$\begin{cases}\Psi_d[k+1] = L_d i_d[k+1] + \Psi_r \\ \Psi_q[k+1] = L_q i_q[k+1]\end{cases} \quad (10)$$

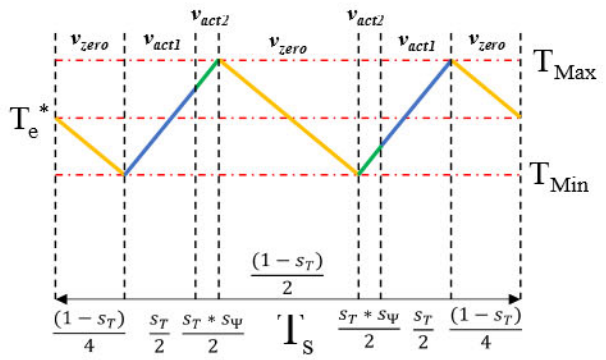

Fig. 5. Illustration of the torque ripple using two active voltage vectors and a zero vector per switching cycle.

In steady state operating conditions, the duty cycle modulation of the inverter results in a seven-step torque waveform similar to that shown in Fig. 5, as would be measured by a perfect torque sensor. These seven steps are simplified into three steps for calculating the torque, currents, and fluxes (6)-(10). The maximum and minimum changes in torque for one control period, ΔT_{Max} and ΔT_{Min}, can be defined in (11). During steady state operation, the difference between ΔT_{Max} and ΔT_{Min} can be minimized to help reduce the torque ripple in one control cycle.

$$\begin{cases} \Delta T_{Max} = \dfrac{T_s\left[s_T s_\Psi \left(\left.\dfrac{dT_e}{dt}\right|_{U_s=v_{act1}}\right) + s_T(1-s_\Psi)\left(\left.\dfrac{dT_e}{dt}\right|_{U_s=v_{act2}}\right)\right]}{2} \\ \Delta T_{Min} = \dfrac{T_s(1-s_T)\left(\left.\dfrac{dT_e}{dt}\right|_{U_s=v_{zero}}\right)}{4} \end{cases} \quad (11)$$

B. Cost Function

The cost function of the MPSDTC is defined by (12), where N is the given prediction horizon, T_e^* is the reference torque, $|\Psi_s|^*$ is the reference flux magnitude, and W_T, W_F, W_I, and W_R are weighting factors of torque, flux, current, and torque ripple, respectively. To increase electrical efficiency, the maximum torque per ampere tracking is implemented in the cost function using the d- and q-axis currents [10]. A discount factor of less than one, γ, increases the impact of output variables closer to those being implemented in the immediate next step. The cost function terms are normalized and then multiplied by individual weights to change their impacts related to the goals of the MPSDTC. Torque is the most important term, so W_T is the largest, followed by W_F, then W_I and W_R. The sum of all the weighting factors is equal to one.

$$\begin{aligned} Cost = \sum_{k=0}^{N} \gamma^k [& W_T\left(T_e^* - (T_e + \Delta T[k])\right)^2 \\ & + W_\Psi\left(|\Psi_s^*[k]| - \sqrt{\Psi_d^2[k] + \Psi_q^2[k]}\right)^2 \\ & + W_I\left(i_d[k] + \frac{L_d - L_q}{\Psi_r}\left(i_d^2[k] - i_q^2[k]\right)\right)^2 \\ & + W_R(\Delta T_{Max}[k] - \Delta T_{Min}[k])^2] \end{aligned} \quad (12)$$

Table II. Electric Machine Parameters

Rated power	180 W
Maximum speed	3000 rpm
Maximum torque	1.9 N·m
V_{dc}	41.75 V
Rated current	7.85 A
R_s	0.235 Ω
L_d	0.275 mH
L_q	0.364 mH
Pole pairs	4

IV. Simulation Results

Three control strategies FOC, SDTC, and MPSDTC were simulated using Matlab/Simulink to control a PMSM with the parameters shown in Table II. The PMSM was operating in torque control mode while a prime mover set the mechanical operating speed at 100, 1000, and 1500 rpm. With a control period of 100 µs, each control strategy was simulated for a step response of 0.75 N·m and steady state performance at 0.75 N·m. The MPSDTC simulation has a prediction horizon of 1, meaning it predicts torque, current, flux, etc. for the immediate next time step and one future time step. The torque is determined from an ideal current sensor and machine parameters sampled at a discrete simulation time step of 1 µs, resulting in the jagged torque waveforms in Figs. (6) and (7).

All three control strategies have parameters that need tuned. The FOC method has three PI controllers, two in the "current loop" and one in the "speed" or "torque loop" in this case. The gains in the PI controllers in the FOC current loops were determined using a bandwidth of 2000 Hz and machine parameters of the PMSM in accordance to [11]. The gains of the PI controller in the outer loop were heuristically tuned at each operating speed to produce sufficient transient response and minimal steady state ripple, favoring transient response. The torque bandwidth and flux bandwidth of the adaptive saturation controllers were heuristically tuned to produce the least amount of steady state ripple since the transient response is already acceptable. The weights in the cost function of the MPSDTC were manually tuned to produce acceptable transient response, steady state ripple, and current THD. Tuning for a reduced steady state ripple can increase the current THD, and vice-versa. The resulting cost function weights were used

The step response transient performance is shown in Fig. 6. For all operating speeds, the MPSDTC reaches the reference the fastest, followed by the SDTC then the FOC. The MPSDTC transient response consistently takes close to 200 µs, or 2 control cycles, to reach the reference for any operating speed. The SDTC similarly takes close to 280 µs, or just under 3 control cycles, to reach the reference at any operating speed. The FOC takes 320 µs at 100 rpm and close to 420 µs at 1000 and 1500 rpm to reach the reference. The results are shown in Table III.

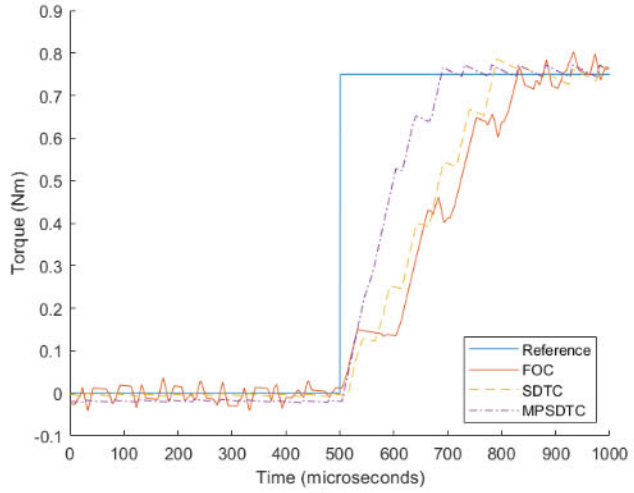

(a)

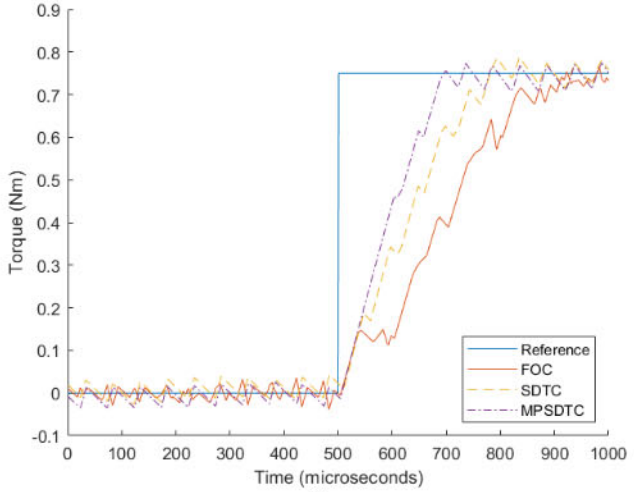

(b)

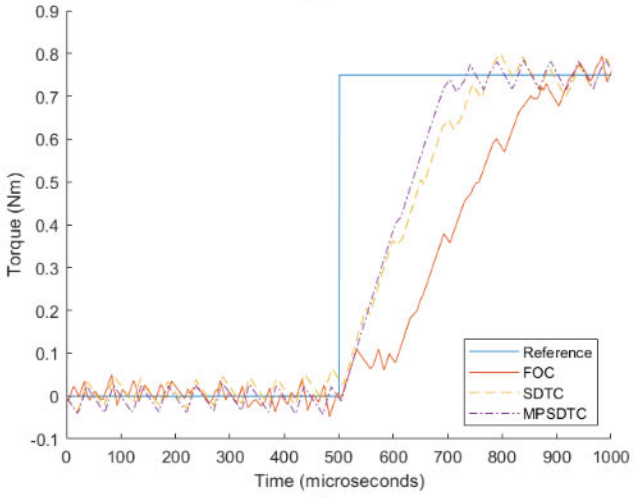

(c)

Fig. 6. Simulated torque step response of FOC, SDTC, and MPSDTC at: (a) 100 rpm, (b) 1000 rpm, and (c) 1500 rpm.

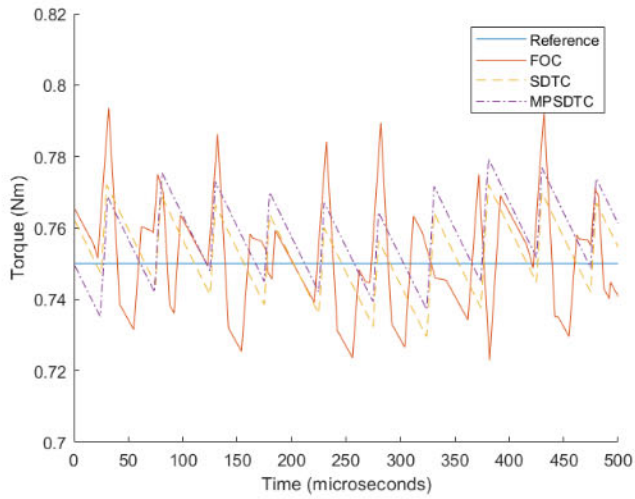

(a)

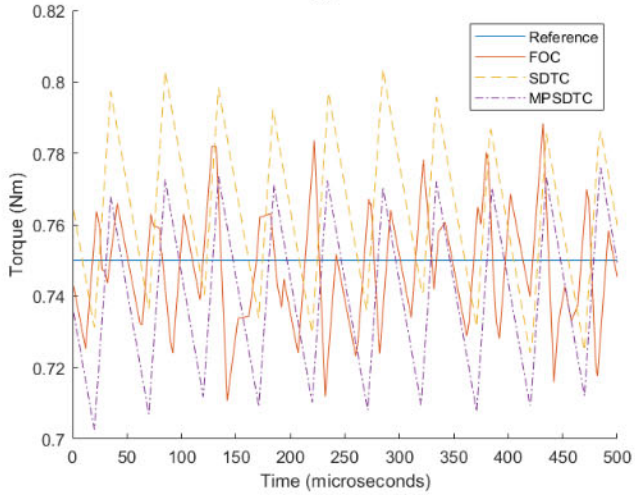

(b)

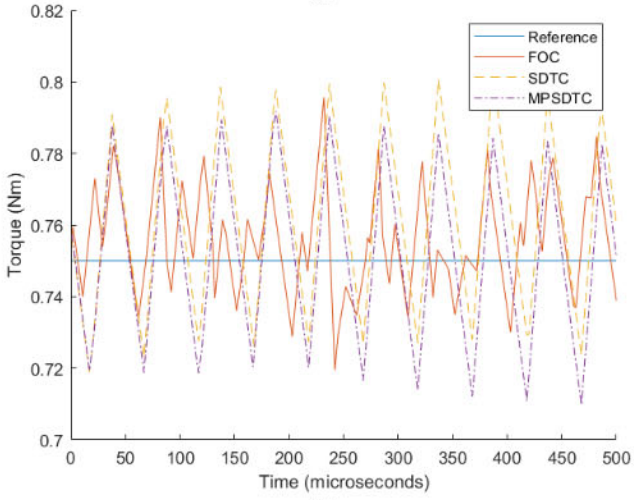

(c)

Fig. 7. Simulated steady state torque of FOC, SDTC, and MPSDTC at: (a) 100 rpm, (b) 1000 rpm, and (c) 1500 rpm.

The steady state performance of 5 control cycles is shown in Fig. 7. The peak to peak torque ripple, mean torque, and current THD are measured over 200 control cycles. At 100 rpm, the FOC has almost double the torque ripple of the

Table III. Simulation Results

RPM	Control Strategy	Rise Time (micro-seconds)	Peak to Peak Torque Ripple (Nm)	Mean Torque Under Load (Nm)	A phase Current THD
100	FOC	326	0.102	0.753	2.89%
	SDTC	281	0.051	0.749	1.80%
	MPSDTC	185	0.047	0.756	3.54%
1000	FOC	420	0.105	0.752	2.78%
	SDTC	276	0.087	0.755	2.74%
	MPSDTC	195	0.078	0.739	2.88%
1500	FOC	421	0.105	0.755	2.91%
	SDTC	271	0.105	0.755	3.58%
	MPSDTC	201	0.092	0.751	3.48%

SDTC and the MPSDTC. This is due to the PI gains being tuned for transient and steady state performance. At 1000 rpm the SDTC has 17% less torque ripple than the FOC, and at 1500 rpm the SDTC and FOC have the same torque ripple. The MPSDTC has 8% to 12% less torque ripple than the SDTC. The MPSDTC also has a slight mean torque offset at 1000 rpm, which shows that slight inaccuracies in the model can result in a mean torque offset. At 100 rpm, the A phase current THD for SDTC is the lowest followed by FOC, due to the PI controller gains tuned favoring transient response. The higher current THD with MPSDTC could be attributed to the cost function favoring torque over flux. At 1000 rpm, the current THD of all control strategies are similar. At 1500 rpm, the SDTC and MPSDTC have a slight increase in current THD. The results are also shown in Table III.

V. Experimental Results

Experimental studies are carried out on an electric motor drive system to verify the transient and steady state results for the FOC, SDTC, and MPSDTC. A block diagram of the experimental platform is shown in Fig. 8 and a picture of the experimental platform is shown in Fig. 9. A PMSM with the same parameters listed in Table II is mechanically coupled to a DC generator operating as the load. The PMSM is driven by a three-phase two-level inverter powered by a DC bus at 41.75 V. The three control schemes are implemented on a dSPACE 1104 real-time control system with a 100 µs control and sampling frequency.

A continuous control sample MPSDTC model was too computationally intensive for the used hardware, so a finite control sample model was substituted. In this model, only the immediate next step is considered, meaning it has a prediction horizon of 0. The values of S_T and S_ψ as calculated in Section II are multiplied with a range of gains from 0.8 to 1.2 to give a range of input vectors. The cost of each of the input vectors is calculated as in Section III. The values of S_T and S_ψ corresponding to the minimal cost are then used to calculate the duty cycle for the control cycle.

The transient results for a 0.75 Nm load step change at 1500 rpm for the FOC, SDTC, and MPSDTC are shown in Fig. 10. The FOC has the slowest response time at 12.9 milliseconds, while the SDTC and the MPSDTC respond at 0.6 milliseconds. The steady state results of a 0.75 Nm load at 1500 rpm for the FOC, SDTC, and MPSDTC for 200 control

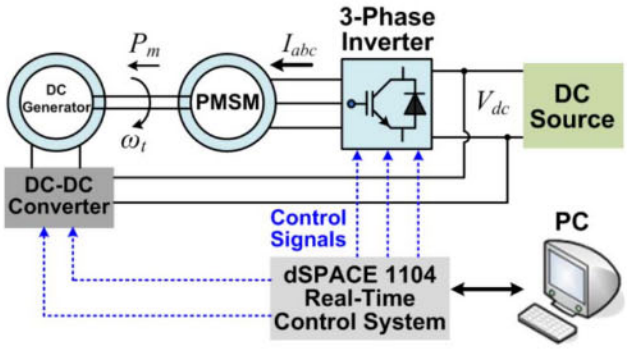

Fig. 8. Block diagram of experimental setup.

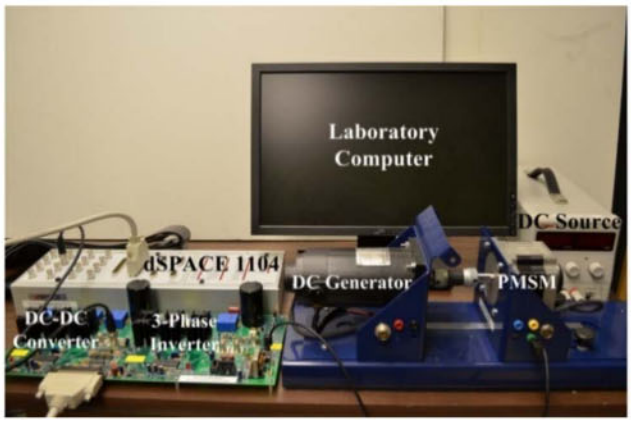

Fig. 9. Picture of experimental setup.

periods are shown in Fig. 10. The SDTC has the highest torque ripple at 0.097 Nm, followed by the FOC at 0.09 Nm, with the MPSDTC having the lowest torque ripple at 0.077 Nm. There is a slight mean offset with the FOC and the MPSDTC. The A phase current THD of the SDTC is the highest at 9.28%, followed by the MPSDTC and the FOC at close to 7.5%.

VI. Conclusion

This paper proposed using MPC to further improve the transient and steady state characteristics of the SDTC. Simulation and experimental results showed the proposed MPSDTC offered a much faster transient response and reduced steady state ripple over the conventional FOC and the SDTC. In simulations with the same control period, the MPSDTC had a 43% to 54% faster step response compared with the FOC and 26% to 34% faster compared with the SDTC. Simulations also showed that the MPSDTC had 25% to 13% lower steady state torque ripple than the FOC and 13% to 8% less ripple than the SDTC.

Experimental results showed that the SDTC had 8% more steady state torque ripple than the FOC, but had a 95% faster step response than the FOC with a PI controller in the outer loop. The MPSDTC retained the fast transient response of the SDTC but reduced the steady state torque ripple of the SDTC by 21%. This results in the MPSDTC having a step transient response 95% faster and a steady state torque ripple 14%

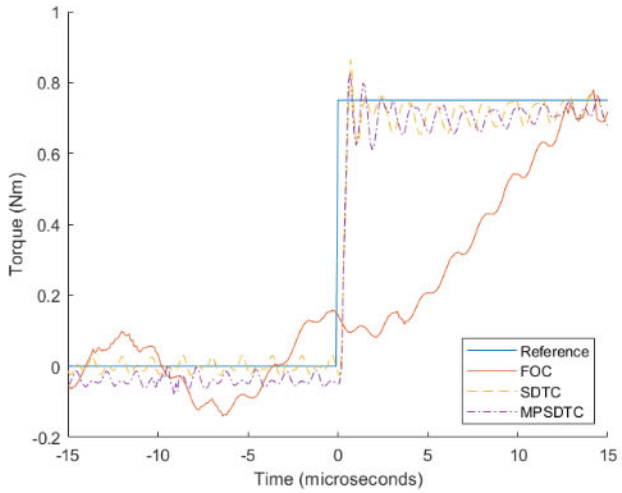

Fig. 10. Experimental torque transient response of the FOC, SDTC, and MPSDTC at 1500 rpm.

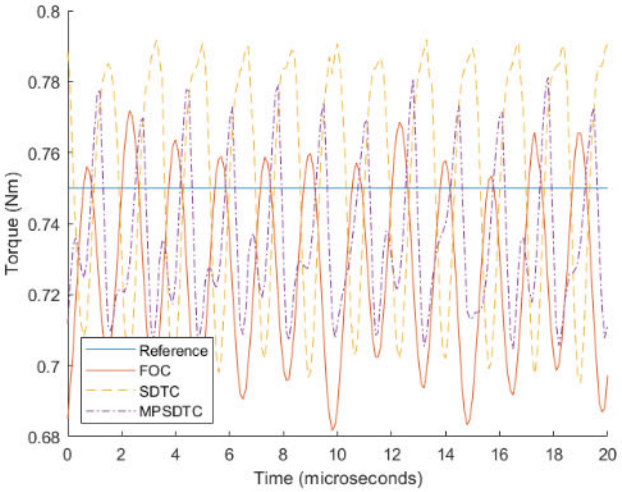

Fig. 11. Experimental steady state torque of the FOC, SDTC, and MPSDTC at 1500 rpm.

Table IV. Experimental Results

Control Strategy	Rise Time (milliseconds)	Peak to Peak Torque Ripple (Nm)	Mean Torque Under Load (Nm)	A phase Current THD
FOC	12.9	0.090	0.717	7.49%
SDTC	0.6	0.097	0.747	9.28%
MPSDTC	0.6	0.077	0.723	7.51%

lower than the conventional FOC with no meaningful change in current THD.

REFERENCES

[1] G. S. Buja and M. P. Kazmierkowski, "Direct torque control of PWM inverter-fed AC motors - A survey," *IEEE Trans. Industrial Electronics*, vol. 51, no. 4, pp. 744-757, Aug. 2004.

[2] D. Casadei, F. Profumo, G. Serra, and A. Tani, "FOC and DTC: two viable schemes for induction motors torque control," *IEEE Trans. Power Electronics*, vol. 17, no. 5, pp. 779-787, Sept. 2002.

[3] C. A. Martins, X. Roboam, T. A. Meynard, and A. S. Carvalho, "Switching frequency imposition and ripple reduction in DTC drives by using a multilevel converter," *IEEE Trans. Power Electronics*, vol. 17, no. 2, pp. 286-297, Mar. 2002.

[4] F. Niu, K. Li, and Y. Wang, "Direct torque control for permanent-magnet synchronous machines based on duty ratio modulation," *IEEE Trans. Industrial Electronics*, vol. 62, no. 10, pp. 6160-6170, Oct. 2015.

[5] T. Geyer, G. Papafotiou, and M. Morari, "Model predictive direct torque control—Part I: Concept, algorithm, and analysis," *IEEE Trans. Industrial Electronics*, vol. 56, no. 6, pp. 1894-1905, Jun. 2009.

[6] Z. Zhou, C. Xia, T. Shi, and Q. Geng, "Model predictive direct duty-cycle control for PMSM drive systems with variable control-set," *IEEE Trans. Industrial Electronics*, Mar. 2020, early access.

[7] Z. Zhang, C. Wei, W. Qiao, and L. Qu, "Adaptive saturation controller-based direct torque control for permanent-magnet synchronous machines," *IEEE Trans. Power Electronics*, vol. 31, no. 10, pp. 7112-7122, Oct. 2016.

[8] L. Qu, L. Qu, W. Qiao, and Z. Zhang, "Zero voltage vector selection in a saturation controller-based direct torque control for permanent-magnet synchronous motors," in *Proc. IEEE Energy Conversion Congress and Exposition*, Sept. 2019, pp. 4528-4533.

[9] S. Lv and H. Lin, "Model predictive direct torque control for PMSM with duty cycle optimization," in *Proc. Fifth International Conference on Instrumentation and Measurement, Computer, Communication and Control*, Sept. 2015, pp. 866-87.

[10] M. Preindl and S. Bolognani, "Model predictive direct torque control with finite control set for PMSM drive systems, Part 1: Maximum torque per ampere operation," *IEEE Trans. Industrial Informatics*, vol. 9, no. 4, pp. 1912-1921, Nov. 2013.

[11] K. J. Astrom and T. Hagglund, *Advanced PID Control*. Research Triangle, NC, USA: Instrumentation, Syst., Automation Society, 2006.